Soft Matter

Cite this: *Soft Matter*, 2012, **8**, 5532

www.rsc.org/softmatter

PAPER

Photoresponsive side-chain liquid crystalline polymers with amide group-substituted azobenzene mesogens: effects of hydrogen bonding, flexible spacers, and terminal tails†

Xinjuan Li, Liangjing Fang, Leigang Hou, Lirong Zhu, Ying Zhang, Baolong Zhang and Huiqi Zhang*

Received 21st January 2012, Accepted 13th March 2012
DOI: 10.1039/c2sm25163a

The synthesis of a series of new photoresponsive side-chain liquid crystalline polymethacrylates with amide group-substituted azobenzene (azo) mesogens and different length of flexible spacers and terminal tails *via* conventional free radical polymerization is described. The resulting azo polymers proved to have high thermal stability and good solubility in common organic solvents (*e.g.*, tetrahydrofuran and chloroform). Differential scanning calorimetry, polarizing optical microscopy, and small angle X-ray scattering studies confirmed the presence of obvious enantiotropic smectic C liquid crystalline phases (with a bilayer lamellar structure) for all these polymers. The introduction of an amide group into the azo mesogen led to the formation of strong hydrogen bonding among the side chains of the polymers (as revealed by variable temperature FT-IR), which played a decisive role in forming and stabilizing the liquid crystalline mesophases of the polymers. In addition, the length of the flexible spacers and terminal tails also significantly influenced their phase transition behaviors. Furthermore, the photoresponsivity of the polymer solutions was verified and the effects of the molecular structures of the polymers on their photoresponsive properties were also studied.

Introduction

Azobenzene (azo)-containing liquid crystalline polymers (LCPs) have received great attention in recent years because of their combined properties of anisotropic liquid crystals, photoresponsive materials, and flexible polymers.[1–12] The liquid crystalline properties of azo polymers are related to the rod-like *trans*-azo mesogens, and the photoinduced fast and reversible isomerization between the *trans* and *cis* isomers of the azo groups upon exposure to UV or visible light provides them with fascinating photoresponsive properties, which can lead to photoinduced reorientation of azo groups in the polymers and triggers significant changes in their physicochemical properties. Many potential applications have been proposed for these polymers, such as optical data storage, liquid crystal displays, molecular switches, nonlinear optical devices, and photomechanical systems. So far, a great number of azo-containing LCPs have been developed for different purposes, including side-chain LCPs with azo mesogens as side groups,[1,3,4,6,7,12] photoresponsive LCPs with azo units located in the main chains,[2,10] and photoresponsive LCP networks.[5,8,10,11] Among them, side-chain LCPs with pendant azo side groups have been the most extensively investigated system.[1,3,4,6,7,12] One of the main focuses in this rapidly developing area is the rational design and efficient synthesis of novel azo-containing side-chain LCPs in order to provide advanced functional materials with potential applications in desired areas.

In general, the molecular structure of an azo-containing side-chain LCP can be divided into three main parts, *i.e.*, the polymer backbone, the pendant photoactive azo mesogens, and the flexible spacer connecting them. A variety of azo-containing side-chain LCPs with different molecular structures have been prepared *via* various polymerization approaches.[1,3,4,6,7,12–22] Systematic studies on the structure–property relationship of the azo-containing side-chain LCPs have revealed that both their phase transition behaviors and photoresponsive properties are strongly dependent on their polymer backbones,[13,14] the azo mesogens,[15–18] and the length of the flexible spacers.[19–22] Among these influencing factors, the molecular structures of the azo mesogens, especially the terminal substitutent of the azo groups, have been recognized as one of the most important primary factors influencing the properties of the azo polymers because the azo groups act as both the mesogenic and photoresponsive units and their substituents can have significant influence on the dipole

---

Key Laboratory of Functional Polymer Materials (Nankai University), Ministry of Education, Department of Chemistry, Nankai University, Tianjin 300071, P. R. China. E-mail: zhanghuiqi@nankai.edu.cn; Fax: +86-2223507193; Tel: +86-2223507193

† Electronic supplementary information (ESI) available. See DOI: 10.1039/c2sm25163a

moment of the azo chromophores and thus their phase transition and photoresponsive behaviors.[15–18] Therefore, many side-chain LCPs bearing pendant azo mesogens with various substituents such as hydrogen,[23] alkyl,[24,25] perfluoroalkyl,[17] alkyloxy,[15,26,27] chiral alkyloxy,[21,28] nitro,[19,29,30] cyano,[31,32] carboxyl,[33] cinnamoyl,[34,35] and *N*-hydroxysuccinimide carboxylate groups[36] have been developed for different purposes.

Recent years have also witnessed considerable interest in the use of hydrogen bonding interaction for the design of various advanced functional polymeric materials.[37–39] In particular, the hydrogen bonding interaction has proven to be of crucial importance in the formation and stabilization of the liquid crystalline phases for many polymers.[40–44] For example, the liquid crystalline mesophases of the aromatic–aliphatic poly(ester amides)[40,41] and poly(ester urethanes)[42] proved to be largely affected by their intermolecular hydrogen bonding among amide–amide and amide–ester moieties. In addition, the intramolecular hydrogen bonding formed between the amide groups in the side chains of poly(*N*-propargylamides) bearing pendant azo groups was found to promote the formation of a helical structure and liquid crystalline phases for the polymer solutions.[43] Very recently, the significant influence of hydrogen bonding on the mesophase structures of mesogen-jacketed LCPs with amide side-chain linkages was also reported.[44] Based on the above results, it can be envisioned that the introduction of an amide group into azo mesogens might lead to photoresponsive side-chain LCPs with better stabilized liquid crystalline mesophases and some interesting properties, which should be positive for many potential applications. To our knowledge, however, side-chain LCPs with amide group-substituted azo mesogens have rarely been reported up to now.

Herein, we report the successful synthesis and characterization of a series of new photoresponsive side-chain liquid crystalline polymethacrylates with amide group-substituted azo mesogens and different lengths of flexible spacer and terminal tails (Scheme 1). The effects of the chemical structures of the azo polymers (including the length of the flexible spacers and terminal tails as well as the amide linkages) on their mesophase properties were studied in detail. The results showed that all the above factors showed great influence on the liquid crystalline properties of the polymers. In particular, the incorporation of an amide group into azo mesogens resulted in the formation of strong hydrogen bonding among the side chains of the azo polymers, which proved to play a decisive role in forming and stabilizing their smectic C liquid crystalline phases. In addition, the photoresponsive properties of the azo polymer solutions were also studied.

Experimental

Materials

Tetrahydrofuran (THF, Tianjin Jiangtian Chemicals, China, 99%) was refluxed over sodium and then distilled. *N*,*N*-Dimethylformamide (DMF, Tianjin Jiangtian Chemicals, 99.5%) was dried with anhydrous magnesium sulfate ($MgSO_4$) and then distilled under vacuum. Triethylamine (Tianjin Jiangtian Chemicals, 99%) was dried with anhydrous sodium sulfate (Na_2SO_4) and then distilled. Thionyl chloride (Tianjin Jiangtian Chemicals, 99.5%) was purified by distillation prior to use. Azobisisobutyronitrile (AIBN, Tianjin Jiangtian Chemicals, chemical purity (CP)) was recrystallized from ethanol and stored at −18 °C before use. 4-((4-Hydroxy)phenylazo)benzoic acid, 4-((4-ω-hydroxyalkyloxy)phenylazo)benzoic acid (HAzoA-*m*, $m = 2, 6, 10$), and 4-((4-ω-methacryloyloxyalkyloxy)phenylazo) benzoic acid (MAzoA-*m*, $m = 2, 6, 10$) (Scheme 1) were prepared

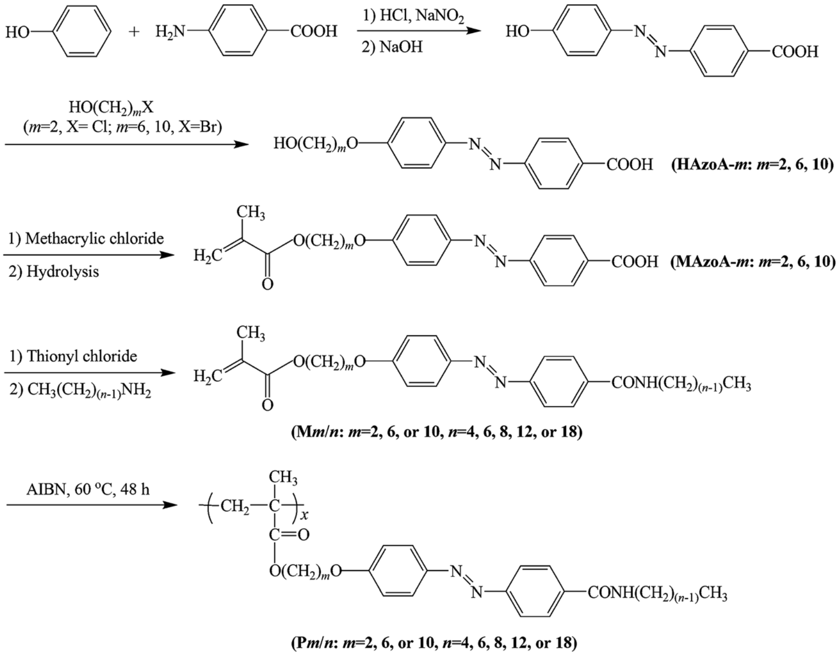

Scheme 1 Synthetic route and chemical structures of the azo monomers M*m*/*n* and their corresponding homopolymers P*m*/*n* ($m = 2$, 6, or 10, $n = 4$, 6, 8, 12, or 18).

according to our previously reported procedure.[36] All the other reagents were commercially available and used as received.

Synthesis of the azo monomers

For convenience, the azo monomers with the amide substitutent were named as M*m*/*n*, where M refers to monomer, *m* the number of the methylene unit in the flexible spacer, and *n* the number of carbon in the terminal alkyl tail (Scheme 1). A series of azo monomers M*m*/*n* ($m = 2$, 6, or 10; $n = 4$, 6, 8, 12, or 18) were synthesized as shown below:

***N*-Hexyl 4-((4-(ω-methacryloyloxyethyloxy))phenylazo)benzamide (M2/6).** MAzoA-2 (0.5 g, 1.20 mmol), DMF (two drops), 2,6-di-*tert*-butylphenol (trace amount), and thionyl chloride (2.5 mL) were added into a three-neck round-bottom flask (25 mL) successively. After the reaction mixture was stirred at room temperature for 4 h, the excessive thionyl chloride was removed at reduced pressure by using a rotoevaporator. The resulting solid was dissolved in dried THF (5 mL) and this solution was added dropwise into a cold mixed solution of *n*-hexamine (0.24 g, 2.40 mmol) and triethylamine (0.8 mL) in dried THF (15 mL). The reaction was allowed to proceed at room temperature for 24 h under stirring and the reaction mixture was filtered. The filtrate was then precipitated into a large amount of water and the resulting solid was filtered, washed with water, and then dried under vacuum at 30 °C for 48 h, leading to the orange-yellow pure product (yield: 90%). UV-vis (THF): λ_{max}/nm (ε/L mol^{-1}cm^{-1}) = 356 (27 980), around 445 (not available due to the overlap of the absorption bands); ^{1}H NMR ($CDCl_3$): δ (ppm) = 7.98–7.85 (m, 6H, Ar–H), 7.06–7.01 (d, 2H, Ar–H), 6.22–6.12 (s,s, 2H, –NH and $CH{=}C-$), 5.61 (s, 1H, $CH{=}C-$), 4.57–4.51 (t, 2H, $-OCH_2-$), 4.36–4.29 (t, 2H, $-CH_2O-$), 3.53–3.43 (quartet (q), 2H, $-NCH_2-$), 1.97 (s, 3H, $-CH_3$), 1.75–0.83 (m, 11H, $-(CH_2)_4CH_3$).

***N*-Butyl 4-((4-(ω-methacryloyloxyhexyloxy))phenylazo)benzamide (M6/4).** Prepared as for M2/6 (yield: 95%). UV-vis (THF): λ_{max}/nm (ε/L mol^{-1}cm^{-1}) = 358 (27 580), around 445 (not available due to the overlap of the absorption bands); ^{1}H NMR ($CDCl_3$): δ (ppm) = 8.02–7.85 (m, 6H, Ar–H), 7.01–6.97 (d, 2H, Ar–H), 6.17 (s, 1H, –NH), 6.10 (s, 1H, $CH{=}C-$), 5.55 (s, 1H, $CH{=}C-$), 4.19–4.15 (t, 2H, $-OCH_2-$), 4.07–4.02 (t, 2H, $-CH_2O-$), 3.53–3.44 (q, 2H, $-NCH_2-$), 1.94 (s, 3H, $-CH_3$), 1.91–0.92 (m, 15H, $-(CH_2)_4$, $-(CH_2)_2CH_3$).

***N*-Hexyl 4-((4-(ω-methacryloyloxyhexyloxy))phenylazo)benzamide (M6/6).** Prepared as for M2/6 (yield: 92%). UV-vis (THF): λ_{max}/nm (ε/L mol^{-1}cm^{-1}) = 358 (26 480), around 445 (not available due to the overlap of the absorption bands); ^{1}H NMR ($CDCl_3$): δ (ppm) = 7.97–7.85 (m, 6H, Ar–H), 7.04–6.97 (d, 2H, Ar–H), 6.16 (s, 1H, –NH), 6.10 (s, 1H, $CH{=}C-$), 5.55 (s, 1H, $CH{=}C-$), 4.21–4.14 (t, 2H, $-OCH_2-$), 4.10–4.02 (t, 2H, $-CH_2O-$), 3.53–3.43 (q, 2H, $-NCH_2-$), 1.95 (s, 3H, $-CH_3$), 1.89–0.86 (m, 19H, $-(CH_2)_4$, $-(CH_2)_4CH_3$).

***N*-Octyl 4-((4-(ω-methacryloyloxyhexyloxy))phenylazo)benzamide (M6/8).** Prepared as for M2/6 (yield: 93%). UV-vis (THF): λ_{max}/nm (ε/L mol^{-1}cm^{-1}) = 358 (28 240), around 445 (not available due to the overlap of the absorption bands); ^{1}H NMR ($CDCl_3$): δ (ppm) = 7.97–7.84 (m, 6H, Ar–H), 7.04–6.96 (d, 2H, Ar–H), 6.17 (s, 1H, –NH), 6.10 (s, 1H, $CH{=}C-$), 5.55 (s, 1H, $CH{=}C-$), 4.19–4.14 (t, 2H, $-OCH_2-$), 4.09–4.01 (t, 2H, $-CH_2O-$), 3.50–3.43 (q, 2H, $-NCH_2-$), 1.94 (s, 3H, $-CH_3$), 1.89–0.83 (m, 23H, $-(CH_2)_4$, $-(CH_2)_6CH_3$)).

***N*-Lauryl 4-((4-(ω-methacryloyloxyhexyloxy))phenylazo)benzamide (M6/12).** Prepared as for M2/6, but the product was purified with silica gel column chromatography by using a mixture of ethyl acetate and petroleum ether (1/2 v/v) as the eluent instead of being directly precipitated into water due to the insolubility of lauryl amine in water (yield: 90%). UV-vis (THF): λ_{max}/nm (ε/L mol^{-1}cm^{-1}) = 358 (26 380), around 445 (not available due to the overlap of the absorption bands); ^{1}H NMR ($CDCl_3$): δ (ppm) = 7.94–7.86 (m, 6H, Ar–H), 7.04–6.96 (d, 2H, Ar–H), 6.17 (s, 1H, –NH), 6.10 (s, 1H, $CH{=}C-$), 5.55 (s, 1H, $CH{=}C-$), 4.21–4.14 (t, 2H, $-OCH_2-$), 4.09–4.02 (t, 2H, $-CH_2O-$), 3.52–3.43 (q, 2H, $-NCH_2-$), 1.95 (s, 3H, $-CH_3$), 1.89–0.83 (m, 31H, $-(CH_2)_4-$, $-(CH_2)_{10}CH_3$).

***N*-Octadecyl 4-((4-(ω-methacryloyloxyhexyloxy))phenylazo)benzamide (M6/18).** Prepared as for M6/12 (yield: 95%). UV-vis (THF): λ_{max}/nm (ε/L mol^{-1}cm^{-1}) = 358 (26 700), around 445 (not available due to the overlap of the absorption bands); ^{1}H NMR ($CDCl_3$): δ (ppm) = 8.07–7.84 (m, 6H, Ar–H), 7.07–6.97 (d, 2H, Ar–H), 6.16 (s, 1H, –NH), 6.10 (s, 1H, $CH{=}C-$), 5.55 (s, 1H, $CH{=}C-$), 4.26–4.13 (t, 2H, $-OCH_2-$), 4.12–4.01 (t, 2H, $-CH_2O-$), 3.54–3.42 (q, 2H, $-NCH_2-$), 1.95 (s, 3H, $-CH_3$), 1.91–0.81 (m, 43H, $-(CH_2)_4-$, $-(CH_2)_{16}CH_3$).

***N*-Hexyl 4-((4-(ω-methacryloyloxydecyloxy))phenylazo)benzamide (M10/6).** Prepared as for M2/6 (yield: 95%). UV-vis (THF): λ_{max}/nm (ε/L mol^{-1}cm^{-1}) = 358 (28 320), around 445 (not available due to the overlap of the absorption bands); ^{1}H NMR ($CDCl_3$): δ (ppm) = 8.16–7.75 (m, 6H, Ar–H), 7.13–6.87 (d, 2H, Ar–H), 6.40–5.98 (s,s, 2H, –NH and $CH{=}C-$), 5.55 (s, 1H, $CH{=}C-$), 4.38–3.88 (m, 4H, $-OCH_2-$ and $-CH_2O-$), 3.65–3.43 (q, 2H, $-NCH_2-$), 1.94 (s, 3H, $-CH_3$), 1.89–0.77 (m, 27H, $-(CH_2)_8-$, $-(CH_2)_4CH_3$).

***N*-Lauryl 4-((4-(ω-methacryloyloxydecyloxy))phenylazo)benzamide (M10/12).** Prepared as for M6/12 (yield: 95%). UV-vis (THF): λ_{max}/nm (ε/L mol^{-1}cm^{-1}) = 358 (27 020), around 445 (not available due to the overlap of the absorption bands); ^{1}H NMR ($CDCl_3$): δ (ppm) = 8.32–8.21 (d, 2H, Ar-H), 8.04–7.86 (m, 4H, Ar-H), 7.13–6.87 (d, 2H, Ar-H), 6.24–6.07 (s, s, 2H, –NH and $CH{=}C-$), 5.55 (s, 1H, $CH{=}C-$), 4.21–4.13 (t, 2H, $-OCH_2-$), 4.11–4.01 (t, 2H, $-CH_2O-$), 3.62–3.40 (q, 2H, $-NCH_2-$), 1.95 (s, 3H, $-CH_3$), 1.91–0.84 (m, 39H, $-(CH_2)_8-$, $-(CH_2)_{10}CH_3$).

In addition to the above azo monomers (M*m*/*n*), another azo monomer named hexyl 4-((4-(ω-methacryloyloxyhexyloxy))phenylazo)benzoate (M6/6-ester) (Scheme S1, Fig. S1a†), which has a similar chemical structure to that of M6/6, but with an ester linkage instead of an amide linkage in the terminal substitutent of the azo mesogen, was also synthesized similarly (yield: 86%). UV-vis (THF): λ_{max}/nm (ε/L mol^{-1}cm^{-1}) = 362 (23 960), around 450 (not available due to the overlap of the absorption bands); ^{1}H NMR ($CDCl_3$): δ (ppm) = 8.22–8.14 (d, 2H, Ar–H), 7.98–7.87

(dd, 4H, Ar–H), 7.05–6.97 (d, 2H, Ar–H), 6.10 (s, 1H, CH=C–), 5.55 (s, 1H, CH=C–), 4.40–4.31 (t, 2H, –OCH_2–), 4.21–4.13 (t, 2H, –OCH_2–), 4.10–4.01 (t, 2H, –CH_2O–), 1.95 (s, 3H, –CH_3), 1.90–0.70 (m, 19H, –$(CH_2)_4$–, –$(CH_2)_4CH_3$).

Synthesis of the azo polymers

For convenience, the side-chain LCPs with the amide group-substituted azo mesogens were named as P*m*/*n*, where P refers to polymer, *m* the number of the methylene unit in the flexible spacer, and *n* the number of carbon in the terminal alkyl tail (Scheme 1). A series of azo polymers P*m*/*n* (*m* = 2, 6, or 10; *n* = 4, 6, 8, 12, or 18) were synthesized following the typical procedure shown below:

The azo monomer M*m*/*n* (0.5 g), AIBN (2 mol% with respect to the monomer), and the freshly distilled DMF (5 mL) were added into a two-neck round-bottom flask. A clear solution was obtained after 10 min of stirring, which was subsequently degassed with three freeze–pump–thaw cycles. The flask was then sealed and immersed into a thermostatted oil bath at 60 °C and stirred for 48 h. After being cooled to the room temperature, the polymerization mixture was added dropwise into ethanol (100 mL) under stirring. The precipitate was collected by filtration, washed with warm ethanol extensively until no azo monomer was detectable by thin layer chromatography, and then dried under vacuum at 60 °C for 48 h to provide the desired orange-yellow polymer (Table 1).

The polymer of M6/6-ester (*i.e.*, P6/6-ester, orange-yellow color) was also prepared similarly following the above procedure (Table 1).

Characterization

^1H NMR spectra were recorded on a Varian Unity plus-400 spectrometer (400 MHz) at ambient temperature. The molecular weights and molecular weight distributions of the polymers were determined with a gel permeation chromatograph (GPC) equipped with a Waters 717 autosampler, a Waters 1525 HPLC pump, three Waters UltraStyragel columns with 5k-600k, 500–30k, and 100–10k molecular ranges, and a Waters 2414 refractive index detector. THF was used as the eluent at a flow rate of 1.0 mL min^{-1}. The calibration curve was obtained using polystyrene (PS) standards. Thermogravimetric analyses (TGA) were performed on a Netzsch TG 209 instrument in a nitrogen atmosphere at a heating rate of 10 °C min^{-1}. Differential scanning calorimetry (DSC, Netzsch 204) was utilized to study the phase transitions of the polymers at a heating/cooling rate of 10 °C min^{-1} under nitrogen. The temperature and heat flow scale were calibrated with standard materials including indium (70–190 °C), tin (150–270 °C), zinc (350–50 °C), bismuth (190–310 °C) and mercury (−100–0 °C) in different temperature ranges. The glass transition temperatures (T_g) of the polymers were determined as the midpoints of the step changes of heat capacity, while the phase transition temperatures were measured from the maximum/minimum of the endothermic/exothermic peaks. The liquid crystalline textures of the samples were observed by using an Olympus BX51 polarizing optical microscope (POM) equipped with a Linksys 32 THMSE600 hot stage and a digital camera (Micropublisher 5.0 RTV). Small angle X-ray scattering (SAXS) measurements were carried out on a Bruker NanoSTAR SAXS system using Cu Ka (λ = 1.542 Å) as the radiation source. The working voltage and current are 40 kV and 35 mA, respectively. The distance between the sample and the detector is 26.55 cm. A temperature control unit in conjunction with the instrument was used to study the structure evolution of liquid crystalline mesophases by heating the samples to the desired temperatures. A Bio-Rad FTS6000 FT-IR spectrometer equipped with an UMA-500 microscope, an MCT detector (cooled with liquid nitrogen), and a Linkam FTIR600

Table 1 Synthetic and characterization data of the azo polymers[a]

Azo polymer	Yield (%)	$M_{n,GPC}$[b] ($\times 10^{-4}$)	PDI[b]	Phase transition[c] T/°C	ΔH[g]/J g^{-1}	T_d[h]/°C
P2/6	56	1.95	1.73	G–S_C 234 I[d,e] I 222 S_C–G[e,f]	16.9 −13.2	327
P6/4	66	2.19	1.75	G 141 S_C 159 I[d] I 146 S_C-G[e,f]	22.4 −20.1	333
P6/6	65	2.97	1.59	G 144 S_C 179 I[d] I 168 S_C-G[e,f]	17.1 −25.7	333
P6/8	63	2.56	1.59	G 141 S_C 196 I[d] I 187 S_C–G[e,f]	20.0 −20.6	341
P6/12	70	2.56	1.59	G 129 S_C 206 I[d] I 196 S_C–G[e,f]	20.1 −19.7	342
P6/18	46	2.74	1.92	G 117 S_C 206 I[d] I 199 S_C 110 G[f]	10.1 −7.7	333
P10/6	66	2.87	1.63	G 136 S_C 154 I[d] I 147 S_C 136 G[f]	32.2 −5.2	332
P10/12	66	2.87	2.53	G 152 S_C 174 I[d] I 164 S_C 138 G[f]	11.2 −13.7	334
P6/6-ester	47	1.64	1.83	G–S_A 82 I[e,d] I 76 S_A–G[e,f]	5.9 −7.3	316

[a] All the azo polymers were prepared *via* the conventional free radical polymerizations of the corresponding azo monomers in DMF with AIBN (2 mol% with respect to the monomer) as the initiator at 60 °C for 48 h. [b] The number-average molecular weights ($M_{n,GPC}$) and polydispersity indices (PDI) of the polymers were determined by GPC with THF as the eluent and PS standards. [c] G, glassy; S_C, smectic C; S_A, smectic A; I, isotropic. [d] Determined with DSC at the second heating scan under nitrogen (10 °C min^{-1}). [e] No T_g was detectable. [f] Determined with DSC at the first cooling scan under nitrogen (−10 °C min^{-1}). [g] ΔH represents the enthalpy of the phase transition. [h] The temperatures at 5% weight loss of the samples under nitrogen were measured by TGA heating experiments at a rate of 10 °C min^{-1}.

hot stage and temperature control system was utilized to carry out the variable temperature FT-IR measurements. The polymer samples were sandwiched between two KBr slides and their temperatures were changed at a rate of 10 °C min^{-1} unless otherwise stated. 16 scans were conducted for each spectrum at the selected temperatures in the wavelength range of 700–4000 cm^{-1} with a resolution of 8 cm^{-1}. A UV-vis scanning spectrophotometer (TU1900, Beijing Purkinje General Instrument Co., Ltd) was utilized to obtain the UV-vis spectra of the monomer and polymer samples at 25 °C. The photochemical isomerization of the azo polymer solutions in THF was investigated by irradiating them first with a 365 nm UV lamp (12 W) until the photostationary state was reached and then with a 450 nm visible light lamp (18 W, wavelength range: 400–550 nm, $\lambda_{\max} = 450$ nm, a filter was put between the samples and the lamp during the study in order to block the light with wavelength $\lambda < 430$ nm). Note that all the above photoresponsive studies were performed by using the same quartz sample cell (with 1 cm pathlength) for the polymer solutions (*i.e.*, the sample thickness is same for all the polymer solutions) and the same incident light intensity (by fixing the distance between the lamps and the samples) in order to accurately evaluate the effects of the molecular structures of the polymers on their photoresponsive properties.

Results and discussion

Synthesis of the amide group-substituted azo monomers and their polymers

A series of new methacrylate azo monomers with the amide substitutent and different lengths of flexible spacer and terminal alkyl chain (*i.e.*, M*m*/*n*: *m* = 2, 6, or 10; *n* = 4, 6, 8, 12, or 18) were synthesized according to the synthetic route illustrated in Scheme 1. 4-((4-Hydroxy)phenylazo)benzoic acid, 4-((4-ω-hydroxyalkyloxy)phenylazo)benzoic acid (HAzoA-*m*, *m* = 2, 6, 10), and 4-((4-ω-methacryloyloxyalkyloxy)phenylazo)benzoic acid (MAzoA-*m*, *m* = 2, 6, 10) were prepared according to the previously reported procedure.[36] MAzoA-*m* (*m* = 2, 6, 10) were reacted with thionyl chloride and the resulting carboxyl chlorides were subsequently coupled with various alkyl amines to provide the desired products M*m*/*n* (*m* = 2, 6, or 10; *n* = 4, 6, 8, 12, or 18) in quite good yields (typically above 90%). The purity of the azo monomers was satisfactory, as verified with both thin layer chromatography and ^{1}H NMR.

The ^{1}H NMR spectrum of one representative azo monomer M6/6 is shown in Fig. 1(a), from which the characteristic vinyl proton signals of the methacryloyl group at 5.55 and 6.10 ppm can be seen clearly. In addition, the chemical shifts and peak integrations of all the protons in the azo monomer are in excellent agreement with its expected structure, demonstrating the successful preparation of pure M6/6. The UV-vis spectrum of the solution of M6/6 in THF exhibits one strong absorption band around 358 nm and another very weak one around 445 nm, respectively (Fig. S2 in the ESI†), which are typical for the azo compounds and can be ascribed to the $\pi \rightarrow \pi^*$ and $n \rightarrow \pi^*$ electron transitions of the –N=N– bond, respectively.[45] Similar results were also obtained for other azo monomers.

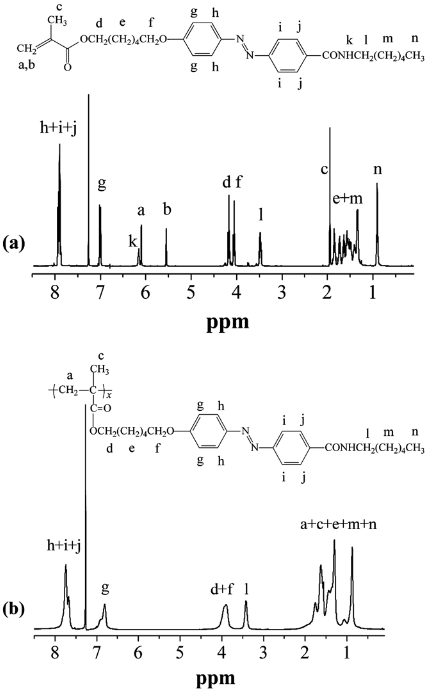

Fig. 1 ^{1}H NMR spectra of M6/6 (a) and P6/6 (b) in CDCl$_3$.

The conventional free radical polymerizations of the azo monomers M*m*/*n* were then carried out with AIBN as the initiator and freshly distilled DMF as the solvent at 60 °C for 48 h with continuous stirring under an argon atmosphere. All the resulting azo polymers (namely P*m*/*n*) were purified by precipitation into ethanol and subsequent thorough washing with warm ethanol until the monomer could no longer be detected by thin layer chromatography . A reasonable polymerization yield of 46–70% was obtained in each case (Table 1). The obtained azo polymers were easily soluble in common organic solvents such as THF, chloroform, and dichloromethane.

The above-obtained azo polymers were firstly characterized with ^{1}H NMR. Fig. 1(b) shows the ^{1}H NMR spectrum of one representative polymer P6/6. It can be seen clearly that the vinyl proton signals of the methacryloyl group from M6/6 have disappeared completely from the spectrum, further confirming that the unreacted azo monomer has been fully removed from the purified polymer. In addition, the chemical shifts and the peak integrations of all the protons in the polymer are in good consistence with its expected structure. Similar results were also obtained for other polymers.

The molecular weights and polydispersity indices (PDI) of the obtained azo polymers P*m*/*n* were determined with GPC and the results are presented in Table 1. It can be seen that the number-average molecular weights $M_{n,\mathrm{GPC}}$ of P*m*/*n* are in the range of 19 500–29 700 and their PDI range from 1.59 to 2.53, which is reasonable for the conventional free radical polymerization of azo-containing methacrylate monomers.[19,21,29,30]

Thermal and phase transition behavior of the azo polymers

The thermal and phase transition behavior of the azo polymers P*m*/*n* were first examined with a combination of TGA, DSC, and

POM. The temperatures at 5% weight loss determined by TGA under nitrogen were found to be ≥327 °C for all these azo polymers, indicating their good thermal stability (Table 1). Fig. 2 shows the DSC curves of the azo polymers with the same length of flexible spacer but with different terminal alkyl chain length (*i.e.*, P6/*n*, $n = 4, 6, 8, 12, 18$). It can be seen clearly that all the azo polymers exhibit one phase transition peak in both the second heating and first cooling scans. In addition, a glass transition at 141, 144, 141, 129, 117 °C was observed for P6/4, P6/6, P6/8, P6/12, and P6/18 in their DSC second heating scan, respectively, revealing that the glass transition temperatures (T_g) of the polymers at first slightly increased with an increase in the length of the terminal alkyl chains from $n = 4$ to 6 and then decreased with a further increase in the terminal tail length, just as reported previously by others.[46] This phenomenon could be ascribed to the combined effects of the steric hindrance and plasticization function of the terminal alkyl chains on the T_g of the polymers. While the steric hindrance effect might be dominant for the polymers with shorter terminal alkyl chains, the plasticization effect might play a more important role for those with longer terminal tails. In this context, it is worth mentioning that the T_g values of P*m*/*n* are obviously higher than those of the previously reported side-chain liquid crystalline polymethacrylates with pendant carboxylate group-substituted azo mesogens,[21,36] which is likely to be due to the formation of hydrogen bonding between the amide groups in these azo polymers. In addition to the glass transition and phase transition, P6/18 also exhibits a faint and rather broad endothermic and exothermic peak around 67 and 58 °C in the DSC second heating and first cooling scans, respectively, which might be caused by the side chain crystallization due to the enhanced flexibility of long terminal tails.[47,48]

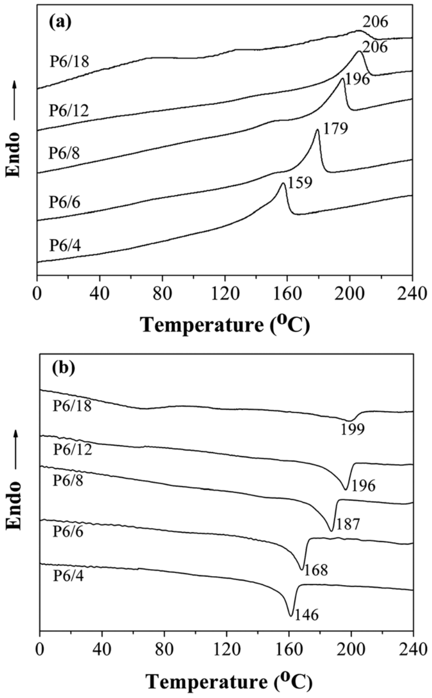

Fig. 2 DSC curves of the azo polymers P6/*n* ($n = 4, 6, 8, 12, 18$) from the second heating scan (a) and from the first cooling scan (b) (±10 °C min^{-1}).

POM study revealed that when the azo polymers P6/*n* ($n = 4, 6, 8, 12, 18$) were cooled from their isotropic states, a large number of anisotropic entities appeared from the dark background of the isotropic liquids and they grew upon further cooling and finally developed into typical schlieren textures (Fig. 3). In addition, POM observations showed that the phase transition peaks in the DSC curves of the azo polymers represented the transition between the liquid crystalline phases and isotropic phases and the mesomorphism was enantiotropic. Furthermore, the liquid crystalline textures of the azo polymers were found to be similar for both the heating and cooling scans. As shown in Table 1, the phase transition temperatures of the azo polymers (*i.e.*, the clearing points T_{cl}) increased markedly when the number of carbon (*i.e.*, *n*) in the terminal alkyl chain increased from 4 to 12, but they levelled off when *n* was further increased. The groups of Jansen[46] and Picken[49] also found that the phase transition temperatures increased with increasing the tail length for a series of side-chain liquid crystalline polycarbonates and polyethers, respectively. In particular, it is noteworthy that the increase in the tail length led to a broader range of liquid crystalline phase (*i.e.*, T_{cl}–T_g) for P6/*n*, which is positive for potential applications.

The DSC curves of the azo polymers with the same length of terminal alkyl chains but different length of flexible spacers (*i.e.*, P*m*/6, $m = 2, 6, 10$) are shown in Fig. 4. It can be seen clearly that the DSC curves of P2/6 and P6/6 exhibit one phase transition peak in both the second heating and first cooling scans. On the other hand, P10/6 shows one phase transition peak in the second

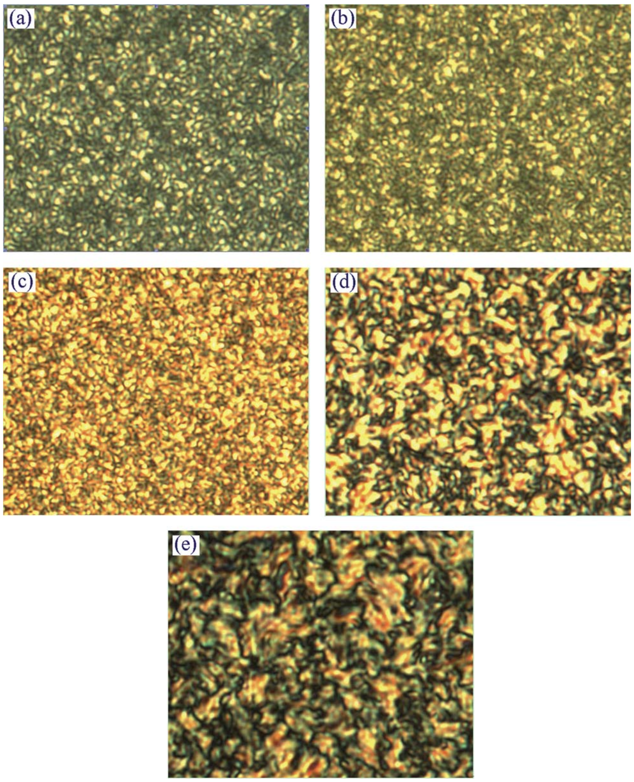

Fig. 3 POM images upon cooling: P6/4 at 144 °C (annealed for 31 min) (a), P6/6 at 166 °C (annealed for 95 min) (b), P6/8 at 185 °C (annealed for 30 min) (c), P6/12 at 194 °C (annealed for 35 min) (d), and P6/18 at 196 °C (annealed for 48 min) (e).

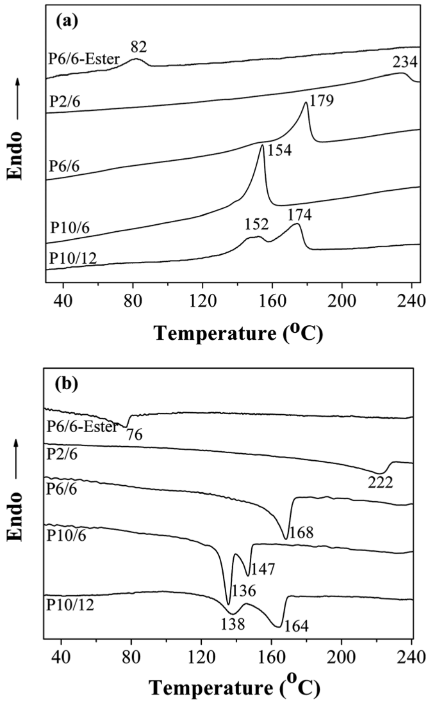

Fig. 4 DSC curves of the azo polymers P6/6-Ester, P*m*/6 (*m* = 2, 6, 10), and P10/12 from the second heating scan (a) and from the first cooling scan (b) (±10 °C min^{-1}).

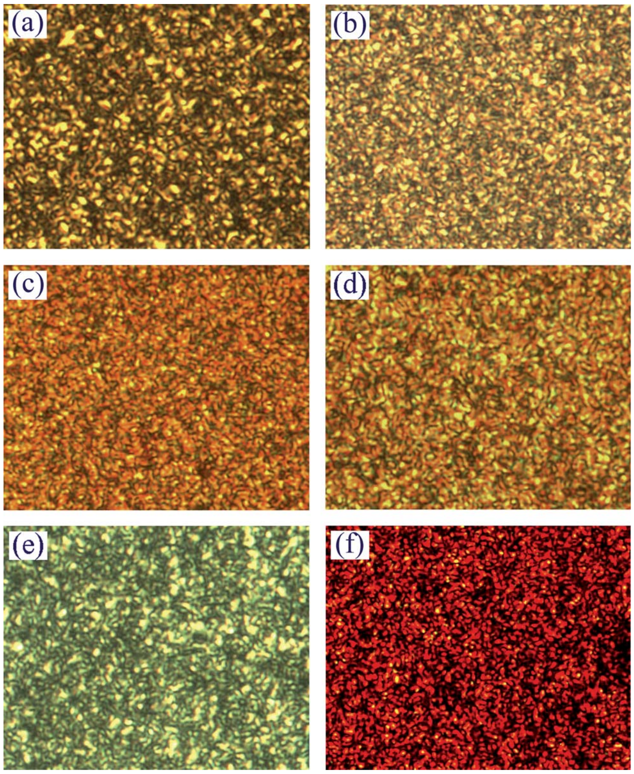

Fig. 5 POM images upon cooling: P2/6 at 220 °C (annealed for 120 min) (a), P6/6 at 166 °C (annealed for 95 min) (b), P10/6 at 144 °C (annealed for 30 min) (c), P10/6 at 134 °C (annealed for 94 min) (d), P10/12 at 160 °C (annealed for 94 min) (e), and P6/6-Ester at 75 °C (annealed for 30 min) (f).

heating scan and two transition peaks in the first cooling scan. No noticeable glass transition was detected for P2/6 in both the second heating and first cooling scans, whereas a glass transition was observed at 144 and 136 °C for P6/6 and P10/6 in the DSC second heating scan, respectively, indicating that the T_g of the polymer series decreased with an increase in the spacer length. This effect has often been observed in side-chain LCPs and has proven to be caused by the increased internal plasticization action with the increase in the spacer length.[21,30] The POM characterization revealed that there existed enantiotropic liquid crystalline phases for all the azo polymers P*m*/6 (*m* = 2, 6, 10) with their mesophases showing schlieren textures (Fig. 5(a–d)). Moreover, the phase transition peaks in the DSC curves of P2/6 and P6/6 in both the second heating and first cooling scans, together with the phase transition peak in the DSC curve of P10/6 in the second heating scan and the higher temperature transition peak in the DSC curve of P10/6 in the first cooling scan, proved to represent the transition between the liquid crystalline phases and isotropic phases. Note that the liquid crystalline textures of P10/6 did not change around the lower temperature transition peak in its DSC curve in the first cooling scan, even after rather long annealing time, indicating that the lower temperature peak did not represent the transition between different liquid crystalline phases (this was further confirmed by the SAXS results in the following part) and it might stem from the glass transition, just as observed by Zhou and coworkers in a series of azo-containing side-chain liquid crystalline poly(1-alkyne)s.[16] To study more about this phenomenon, another azo polymer P10/12 was also synthesized, which has the same length of flexible spacer as P10/6 but with a longer terminal tail. The DSC investigation showed that there existed two peaks in both the first cooling and second heating scans for P10/12 (Fig. 4). A careful study with POM also demonstrated that the higher temperature peaks represented the transition between the liquid crystalline phases and isotropic phases, while the lower temperature ones might be glass transition peaks.

It is well known that SAXS can provide useful information concerning molecular arrangement, packing mode of the mesogen, and type of order in the mesophase of a liquid crystalline polymer and it has thus been widely utilized for accurately assigning the exact nature of the liquid crystalline phases.[36,50,51] Therefore, the liquid crystalline mesophases of some representative azo polymers (*i.e.*, P6/6, P6/12, and P10/6) were further studied with *in situ* variable temperature SAXS. Fig. 6 shows the SAXS patterns of the studied azo polymers, which were obtained at their liquid crystalline temperatures (with a certain time of annealing) upon cooling from the isotropic states. Three scattering peaks at q_1 = 1.23, q_2 = 2.47, and q_3 = 3.70 nm^{-1} were discernible in the SAXS pattern of P6/6 with the ratio of q_1 to q_2 to q_3 being 1 : 2 : 3 (Fig. 6(b)), which demonstrated the presence of a long-range ordered lamellar structure.[51] This, together with its schlieren texture (as observed with POM) and the general rule "schlieren texture is frequently found in the smectic C phase instead of smectic A phase",[44] revealed the presence of a smectic C liquid crystalline phase for P6/6. In addition, three scattering peaks with q_1 = 1.04, q_2 = 2.06, and q_3 = 3.10 nm^{-1} were observed in the SAXS pattern of P6/12 with the ratio of q_1 to q_2

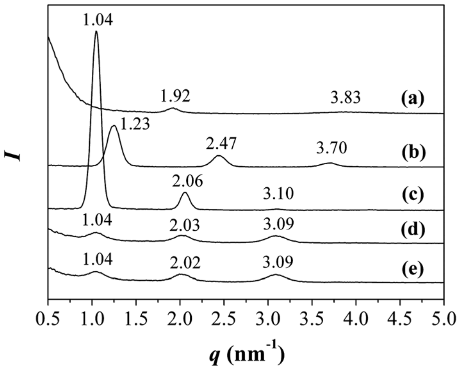

Fig. 6 SAXS patterns of the azo polymers upon cooling from the isotropic states: P6/6-ester at 74 °C with an annealing time of 40 min (scan time: 30 min) (a), P6/6 at 166 °C with an annealing time of 10 min (scan time: 10 min) (b), P6/12 at 194 °C with an annealing time of 10 min (scan time: 10 min) (c), P10/6 at 144 °C with an annealing time of 10 min (scan time: 10 min) (d), and P10/6 at 133 °C with an annealing time of 10 min (scan time: 10 min) (e).

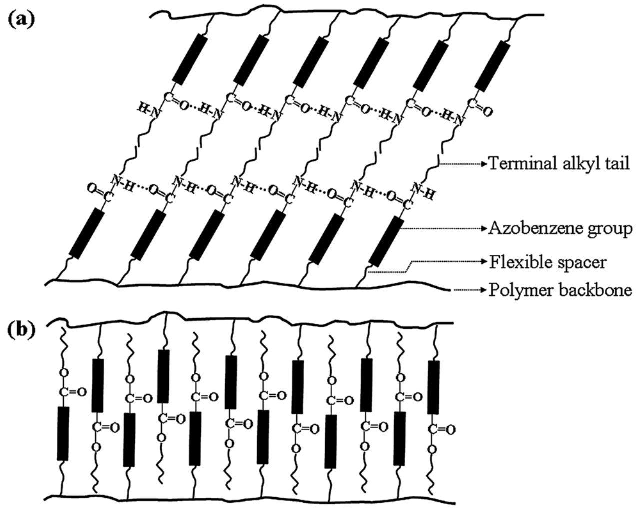

Fig. 7 Possible liquid crystalline mesophase structures of P*m*/*n* (a) and P6/6-ester (b).

to q_3 being 1 : 2 : 3 (Fig. 6(c)), again suggesting the presence of a smectic C liquid crystalline phase for P6/12. Similarly, P10/6 also showed three scattering peaks at q_1 = 1.04, q_2 = 2.03, and q_3 = 3.09 nm^{-1} in its SAXS pattern, with the ratio of q_1 to q_2 to q_3 being 1 : 2 : 3 (Fig. 6(d)). More importantly, no change was observed for the SAXS patterns of P10/6 at both 144 (Fig. 6(d)) and 133 °C (Fig. 6(e)) (even after annealing), which was consistent with the POM result and further confirmed that the lower temperature peak in the DSC first cooling curve of P10/6 did not represent the transition between two liquid crystalline phases. Based on the DSC, POM, and SAXS results, we can conclude that all the obtained azo polymers P*m*/*n* showed enantiotropic smectic C liquid crystalline phases. Table 2 presents the mesophase layer spacing values (*d*) of the above side-chain LCPs determined with SAXS ($d = 2\pi/q_1$).[51] The obtained *d* values proved to be greater than the calculated molecular length (*l*) for the fully extended side-chain liquid crystalline unit of P*m*/*n*, but smaller than 2*l*, suggesting a possible bilayer lamellar structure, as schematically shown in Fig. 7(a), where the hydrogen bonding formed among the neighboring amide groups was considered to enhance the attractive interaction between the mesogenic groups and stabilize the liquid crystalline mesophases.

To confirm the presence of hydrogen bonding among the amide groups in the liquid crystalline phases of P*m*/*n*, their variable temperature FT-IR experiments were performed. It has been well established that the FT-IR spectral peak positions of both the N–H stretching ($\nu_{\text{N–H}}$) and C=O stretching (amide I) bands from the amide groups can provide useful information about their hydrogen bonding state.[44,52,53] Fig. 8 shows the variable temperature FT-IR spectra of the representative polymer P6/6 obtained during both the second heating and first cooling processes. It can be seen clearly that P6/6 exhibits two infrared bands at 3445 cm^{-1} (very weak shoulder) and 3317 cm^{-1} (strong peak) for $\nu_{\text{N–H}}$ at ambient temperature, which can be assigned to the "free" (higher than 3400 cm^{-1}) and hydrogen-bonded N–H stretching modes, respectively. This, together with the rather low-frequency peak of the amide I band (1637 cm^{-1}, C=O stretching), clearly demonstrates that most N–H groups are associated with C=O groups through hydrogen bonding at room temperature. Moreover, the N–H stretching vibration also proved to be dependent on the sample's temperature. The hydrogen-bonded N–H stretching peak (with a frequency lower than 3400 cm^{-1}) became weaker and shifted towards higher frequencies upon increasing the sample temperature, while the free N–H stretching peak with a frequency higher than 3400 cm^{-1} became stronger in the meantime (Fig. 8(a)), indicating that the hydrogen bonding among the amide groups got weaker and some of the bonded N–H groups were transformed to free ones with increasing temperature (it is worth mentioning here, however, that the hydrogen bonding still existed among the

Table 2 SAXS characterization conditions and results of the azo polymers

Azo polymer	T_{analysis} (°C)[a]	$t_{\text{annealing}}$ (min)[a]	*l* (nm)[b]	*d* (nm)[c]	Liquid crystalline mesophase[d]
P6/6	166	10	3.12	5.11	Bilayer S_C
P6/12	194	10	3.87	6.04	Bilayer S_C
P10/6	144	10	3.62	6.04	Bilayer S_C
	133	10	3.62	6.04	Bilayer S_C
P6/6-ester	74	40	3.12	3.27	Fully interdigitated S_A

[a] T_{analysis} and $t_{\text{annealing}}$ refer to the SAXS analysis temperatures and annealing times for the azo polymers during their first cooling processes. [b] The calculated molecular length (*l*) for the fully extended side-chain liquid crystalline units of the studied azo polymers. [c] The mesophase layer spacing of the side-chain LCPs determined by SAXS. [d] S_C, smectic C; S_A, smectic A.

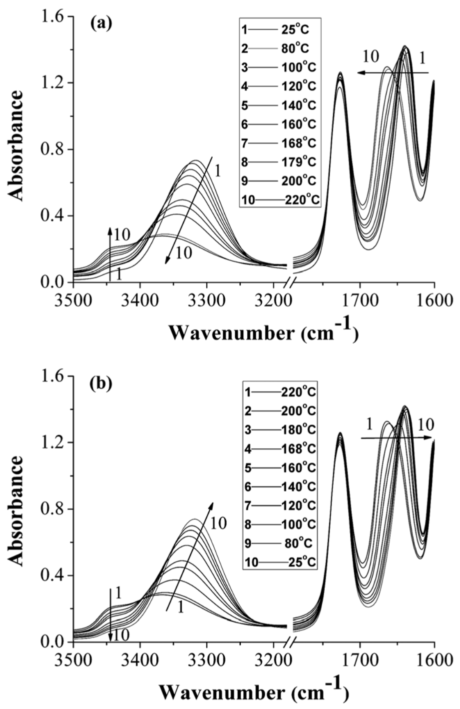

Fig. 8 FT-IR spectra of P6/6 at different temperatures during the second heating (a) and first cooling (b) processes.

amide groups in the polymers even at 220 °C). On the other hand, the intensity and frequency of the N–H stretching vibration were fully recovered upon decreasing the sample temperature, suggesting that the hydrogen bonding interaction was reversible, just as expected (Fig. 8(b)). Note that the C═O stretching band of the amide groups in the studied polymer also showed reversible change in its frequency following the change of the sample temperatures while no frequency shift was observed for the C═O stretching band from the ester groups in the polymer, which further demonstrated the formation of hydrogen bonding between C═O and N–H groups of the amide substitutents in the azo polymer.

To get more insight into the effect of hydrogen bonding on the mesophases of the above azo polymers, a new side-chain LCP named P6/6-ester was also synthesized as a control polymer, which has a similar chemical structure to that of P6/6, but with an ester linkage instead of an amide linkage in the terminal substitutent of the azo mesogen (Scheme S1, Fig. S1b†). Fig. 4 shows the DSC curves of P6/6-ester from both the second heating and first cooling scans. It can be seen clearly that the DSC curves of P6/6-ester exhibit one obvious phase transition peak in both the second heating and first cooling scans, just as P6/6. However, the phase transition temperature of P6/6-ester proved to be significantly lower than that of P6/6 and a temperature difference of 92 (upon the first cooling scan)/97 °C (upon the second heating scan) was observed between P6/6-ester and P6/6, which is likely to be due to the absence of hydrogen bonding among the neighboring azo mesogens in P6/6-ester. POM observation revealed the presence of obvious broken focal-conic textures during both the heating and cooling processes of P6/6-ester (Fig. 5(f)), indicating that the studied polymer had an enantiotropic smectic mesophase. The SAXS pattern of P6/6-ester was obtained at its liquid crystalline temperature (with a certain time of annealing) upon cooling from the isotropic state (Fig. 6(a)), where one weak scattering peak at $q_1 = 1.92\ \text{nm}^{-1}$ and another very weak one at $q_2 = 3.83\ \text{nm}^{-1}$ were detectable with the ratio of q_2 to q_1 being 2, suggesting the presence of a long-range ordered lamellar structure with a layer spacing $d = 3.27$ nm ($d = 2\pi/q_1$).[51] This d value is in good agreement with the calculated molecular length (l) for the fully extended side-chain liquid crystalline unit of P6/6-ester (l = 3.12 nm), suggesting a fully interdigitated smectic A structure (*i.e.*, near to 100% overlap of the side-chain units), as schematically shown in Fig. 7(b). It can thus be concluded on the basis of the above results that the hydrogen bonding interaction indeed plays a decisive role in the formation and stabilization of smectic C liquid crystalline phases in the side-chain LCPs containing amide-substituted azo mesogens.

Photoisomerization behavior of the azo polymers

The photochemical properties of one representative azo polymer P6/6 in THF were firstly investigated. By irradiation with 365 nm UV light, the studied polymer solution underwent *trans* to *cis* photoisomerization until a photostationary state was eventually reached (Fig. 9(a)). The intensity of the $\pi \rightarrow \pi^*$ transition band around 356 nm decreased, whereas the intensity of the $n \rightarrow \pi^*$ transition band around 445 nm slightly increased. The existence of isobestic points at 310 and 417 nm is characteristic for the existence of two distinct absorbing species in equilibrium with each other and at the same time proves that no side reaction takes place during the photoisomerization process in the range studied. Fig. 9(b) shows the UV-vis spectral changes of P6/6 solution in

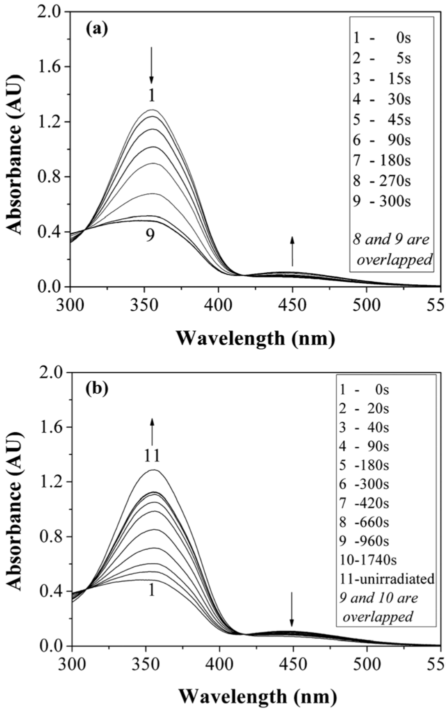

Fig. 9 UV-vis spectral changes in dependence of time for the solution of P6/6 in THF (C = 0.0247 mg mL^{-1}) at 25 °C upon irradiation with 365 nm light (a) and upon irradiating the polymer solution at the photostationary state with λ > 430 nm visible light (b).

THF with time under irradiation with $\lambda > 430$ nm visible light, where the polymer solution had been irradiated with 365 nm UV light for 300 s prior to visible light irradiation. It can clearly be seen that the polymer solution undergoes *cis* to *trans* back-isomerization upon visible light irradiation, but the finally recovered absorbance of *trans*-azobenzene is lower than that before UV irradiation with the recovery of the *trans*-isomer being 87%. A similar phenomenon was also observed previously by us and others.[36,54,55] Its real cause is not totally clear yet but might be that, at the same wavelength where *cis* to *trans* photochemical back-isomerization was performed, there was also a weak absorption from the *trans*-isomer, which eventually led to an equilibrium with *cis* to *trans* and *trans* to *cis* isomerizations taking place under the same visible light after most of the *cis*-isomer returned to the *trans*-isomer.[26,36] Nevertheless, the photochemical isomerization became completely reversible upon the subsequent cycles of UV and visible light irradiation (Fig. not shown).

The time dependence of the relative absorbance (*i.e.*, A_t/A_0, where A_t refers to the absorbance of the polymer solution at 356 nm at time t upon UV or visible light irradiation and A_0 the original absorbance of the polymer solution at 356 nm without UV light irradiation) of the polymer series P6/n (n = 4, 6, 8, 12, 18) in THF showed that the photoinduced isomerization rates of the P6/n solutions were rather similar under the irradiation of 365 nm UV light (Fig. 10(a)). However, the relative absorbance of the P6/18 solution in the photostationary state finally reached proved to be somehow higher than those of the other P6/n (n = 4, 6, 8, 12) solutions. Its real cause is not yet fully understood, but probably due to the entanglement of the rather long terminal alkyl chain in this polymer, thus leading to more restriction to the azo groups during their photochemical isomerization process. Similarly, the photochemical back-isomerization rates of the polymer solutions under the irradiation of visible light were also more or less the same, but the relative absorbance of the P6/18 solution in the photostationary state finally reached was again somehow higher than those of the other P6/n (n = 4, 6, 8, 12) solutions (Fig. 10(b)). Further investigation is underway to provide a reasonable explanation for this phenomenon.

The time dependence of the relative absorbance of the polymer series Pm/6 (m = 2, 6, 10) in THF was also studied (Fig. 11). Fig. 11(a) shows that the polymer with a shorter flexible spacer (*i.e.*, P2/6) had a relatively higher relative absorbance (*i.e.*, lower conversion of *trans*-isomer to *cis*-isomer) under the irradiation of UV light when the photostationary state was eventually reached, which might stem from the more significant coupling effect between the polymer backbones and the pendant azo groups in the presence of a shorter flexible spacer, just as observed by Wang and coworkers for the photoinduced mass-migration behavior of the azo-containing side-chain LCPs with different length flexible spacers.[20] In comparison, the photochemical back-isomerization processes of the Pm/6 solutions under the irradiation of visible light were more or less the same, suggesting that the length of the flexible spacers in the azo polymers has little influence on their visible light-driven back-isomerization processes (Fig. 11(b)).

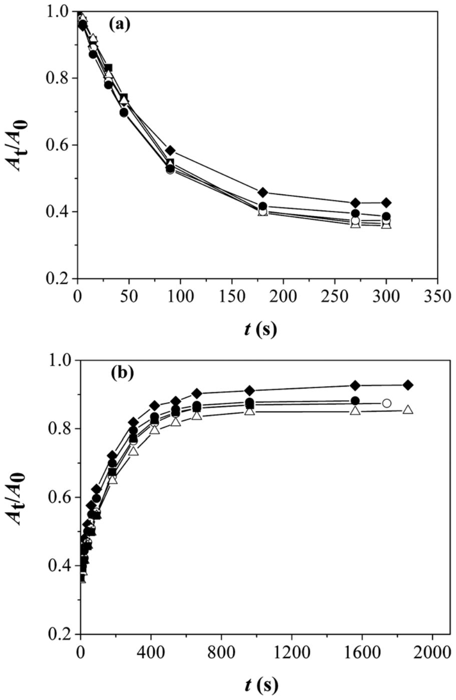

Fig. 10 Dependence of the relative absorbance (A_t/A_0, $\lambda = 356$ nm) on time upon irradiation with 365 nm UV light (a) or with $\lambda > 430$ nm visible light (b) for the P6/n (n = 4 (filled square), 6 (empty circle), 8 (empty triangle), 12 (filled circle), 18 (filled diamond)) solutions in THF (C = 0.0247 mg mL^{-1}) at 25 °C.

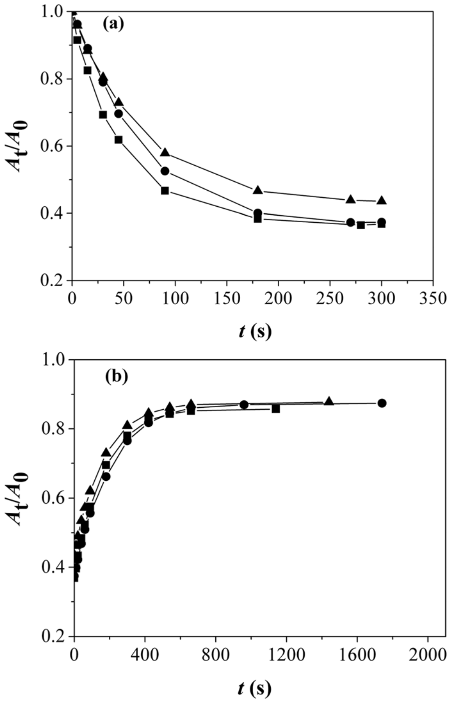

Fig. 11 Dependence of the relative absorbance (A_t/A_0, $\lambda = 356$ nm) on time upon irradiation with 365 nm UV light (a) or with $\lambda > 430$ nm visible light (b) for the Pm/6 (m = 2 (triangle), 6 (circle), 10 (square)) solutions in THF (C = 0.0247 mg mL^{-1}) at 25 °C.

Conclusions

A series of new photoresponsive side-chain liquid crystalline polymethacrylates with amide group-substituted azo mesogens and different length of flexible spacers and terminal alkyl chains have been successfully synthesized *via* conventional free radical polymerization. Hydrogen bonding interactions among the amide groups proved to play a decisive role in forming and stabilizing the smectic C liquid crystalline mesophase structures of the polymers. In addition, the length of the flexible spacers and the terminal tails also showed great influence on the phase transition behavior of the azo polymers in terms of their glass transition and phase transition temperatures, where the increase in the tail length led to a broader range of liquid crystalline phase for the azo polymers, which is positive for potential applications. Furthermore, the photoresponsivity of the polymer solutions was also confirmed by the occurrence of the UV and visible light-induced *trans*/*cis* photoisomerization. We believe that the introduction of an amide substitutent into the pendant azo mesogens of the polymers opens up a new avenue for efficiently designing and controlling the liquid crystalline mesophase structures of the azo side-chain LCPs and the resulting novel amide group-substituted azo LCPs with a broad range of stable liquid crystalline phases and obvious photoresponsive properties are highly promising for many potential applications.

Acknowledgements

The authors gratefully acknowledge the financial supports from the National Natural Science Foundation of China (20974048), Natural Science Foundation of Tianjin (06YFMJC15100, 11JCYBJC01500), and a Start-up Fund from Nankai University.

References

1 H. Zhang, C. Li, W. Huang and B. He, *Chinese Polym. Bull.*, 1998, 63–69.
2 N. K. Viswanathan, D. Y. Kim, S. Bian, J. Williams, W. Liu, L. Li, L. Samuelson, J. Kumar and S. K. Tripathy, *J. Mater. Chem.*, 1999, **9**, 1941–1955.
3 A. Natansohn and P. Rochon, *Chem. Rev.*, 2002, **102**, 4139–4175.
4 T. Ikeda, *J. Mater. Chem.*, 2003, **13**, 2037–2057.
5 Y. Yu, M. Nakano and T. Ikeda, *Nature*, 2003, **425**, 145.
6 V. Shibaev, A. Bobrovsky and N. Boiko, *Prog. Polym. Sci.*, 2003, **28**, 729–836.
7 Y. Zhao, *Pure Appl. Chem.*, 2004, **76**, 1499–1508.
8 P. Xie and R. Zhang, *J. Mater. Chem.*, 2005, **15**, 2529–2550.
9 M. H. Li and P. Keller, *Philos. Trans. R. Soc. London, Ser. A*, 2006, **364**, 2763–2777.
10 T. Ikeda, J. I. Mamiya and Y. Yu, *Angew. Chem., Int. Ed.*, 2007, **46**, 506–528.
11 C. Ohm, M. Brehmer and R. Zentel, *Adv. Mater.*, 2010, **22**, 3366–3387.
12 J. M. Schumers, C. A. Fustin and J. F. Gohy, *Macromol. Rapid Commun.*, 2010, **31**, 1588–1607.
13 M. Han, M. Kidowaki, K. Ichimura, P. S. Ramanujam and S. Hvilsted, *Macromolecules*, 2001, **34**, 4256–4262.
14 J. Isayama, S. Nagano and T. Seki, *Macromolecules*, 2010, **43**, 4105–4112.
15 X. Tang, L. Gao, X. Fan and Q. Zhou, *J. Polym. Sci., Part A: Polym. Chem.*, 2007, **45**, 5190–5198.
16 J. L. Zhou, X. F. Chen, X. H. Fan, C. P. Chai, C. X. Lu, X. D. Zhao, Q. W. Pan, H. Y. Tang, L. C. Gao and Q. F. Zhou, *J. Polym. Sci., Part A: Polym. Chem.*, 2006, **44**, 4532–4545.
17 F. You, M. Y. Paik, M. Häckel, L. Kador, D. Kropp, H. W. Schmidt and C. K. Ober, *Adv. Funct. Mater.*, 2006, **16**, 1577–1581.
18 Z. Zheng, Z. Su, L. Wang, J. Xu, Q. Zhang and J. Yang, *Eur. Polym. J.*, 2007, **43**, 2738–2744.
19 S. Freiberg, F. Lagugné-Labarthet, P. Rochon and A. Natansohn, *Macromolecules*, 2003, **36**, 2680–2688.
20 D. Wang, G. Ye, Y. Zhu and X. Wang, *Macromolecules*, 2009, **42**, 2651–2657.
21 Z. Zheng, J. Xu, Y. Sun, J. Zhou, B. Chen, Q. Zhang and K. Wang, *J. Polym. Sci., Part A: Polym. Chem.*, 2006, **44**, 3210–3219.
22 S. Hvilsted, F. Andruzzi, C. Kulinna, H. W. Siesler and P. S. Ramanyjam, *Macromolecules*, 1995, **28**, 2172–2183.
23 A. Böhme, J. Lindau, U. Rötz, F. Hoffmann, H. Fischer, S. Diele and F. Kuschel, *Makromol. Chem.*, 1992, **193**, 2581–2588.
24 Q. Bo, A. Yavrian, T. Galstian and Y. Zhao, *Macromolecules*, 2005, **38**, 3079–3086.
25 H. Yu, J. Li, T. Ikeda and T. Iyoda, *Adv. Mater.*, 2006, **18**, 2213–2215.
26 M. H. Li, P. Keller, B. Li, X. Wang and M. Brunet, *Adv. Mater.*, 2003, **15**, 569–572.
27 X. Tong, L. Cui and Y. Zhao, *Macromolecules*, 2004, **37**, 3101–3112.
28 A. Yu. Bobrovsky, N. I. Boiko and V. P. Shibaev, *Chem. Mater.*, 2001, **13**, 1998–2001.
29 H. Zhang, W. Huang, C. Li and B. He, *Eur. Polym. J.*, 1998, **34**, 1521–1529.
30 C. Cojocariu and P. Rochon, *Macromolecules*, 2005, **38**, 9526–9538.
31 H. Yu, T. Iyoda and T. Ikeda, *J. Am. Chem. Soc.*, 2006, **128**, 11010–11011.
32 P. Forcén, L. Oriol, C. Sánchez, R. Alcalá, S. Hvilsted, K. Jankova and J. Loos, *J. Polym. Sci., Part A: Polym. Chem.*, 2007, **45**, 1899–1910.
33 H. J. Haitjema, R. Buruma, G. O. R. Alberda van Ekenstein, Y. Y. Tan and G. Challa, *Eur. Polym. J.*, 1996, **32**, 1447–1455.
34 H. W. Gu, P. Xie, D. Y. Shen, P. F. Fu, J. M. Zhang, Z. R. Shen, Y. X. Tang, L. Cui, B. Kong, X. F. Wei, Q. Wu, F. L. Bai and R. B. Zhang, *Adv. Mater.*, 2003, **15**, 1355–1358.
35 H. W. Gu, P. Xie, P. F. Fu, T. Y. Zhang and R. B. Zhang, *Adv. Funct. Mater.*, 2005, **15**, 125–130.
36 X. Li, R. Wen, Y. Zhang, L. Zhu, B. Zhang and H. Zhang, *J. Mater. Chem.*, 2009, **19**, 236–245.
37 W. H. Binder and R. Zirbs, in *Hydrogen Bonded Polymers*, Springer-Verlag, Berlin, 2007, 207, 1–78.
38 L. Brunsveld, B. J. B. Folmer, E. W. Meijer and R. P. Sijbesma, *Chem. Rev.*, 2001, **101**, 4071–4097.
39 H. Zhang, L. Ye and K. Mosbach, *J. Mol. Recognit.*, 2006, **19**, 248–259.
40 N. S. Murthy and S. M. Aharoni, *Macromolecules*, 1992, **25**, 1177–1183.
41 J. D. Sudha and C. K. S. Pillai, *J. Polym. Sci., Part A: Polym. Chem.*, 2003, **41**, 335–346.
42 F. S. Yen, L. L. Lin and J. L. Hong, *Macromolecules*, 1999, **32**, 3068–3079.
43 T. Fujii, M. Shiotsuki, Y. Inai, F. Sanda and T. Masuda, *Macromolecules*, 2007, **40**, 7079–7088.
44 Y. H. Cheng, W. P. Chen, Z. Shen, X. H. Fan, M. F. Zhu and Q. F. Zhou, *Macromolecules*, 2011, **44**, 1429–1437.
45 M. Niemann and H. Ritter, *Makromol. Chem.*, 1993, **194**, 1169–1181.
46 J. C. Jansen, R. Addink, K. te Nijenhuis and W. J. Mijs, *Macromol. Chem. Phys.*, 1999, **200**, 1473–1484.
47 S. K. Ahn, L. T. N. Le and R. M. Kasi, *J. Polym. Sci., Part A: Polym. Chem.*, 2009, **47**, 2690–2701.
48 C. Pugh and A. L. Kiste, *Prog. Polym. Sci.*, 1997, **22**, 601–691.
49 J. B. Reesink, S. J. Picken, A. J. Witteveen and W. J. Mijs, *Macromol. Chem. Phys.*, 1996, **197**, 1031–1041.
50 Z. Li, Y. Zhang, L. Zhu, T. Shen and H. Zhang, *Polym. Chem.*, 2010, **1**, 1501–1511.
51 X. F. Chen, K. K. Tenneti, C. Y. Li, Y. Bai, X. Wan, X. Fan, Q. F. Zhou, L. Rong and B. S. Hsiao, *Macromolecules*, 2007, **40**, 840–848.
52 D. J. Skrovanek, S. E. Howe, P. C. Painter and M. M. Coleman, *Macromolecules*, 1985, **18**, 1676–1683.
53 C. Xue, S. Jin, X. Weng, J. J. Ge, Z. Shen, H. Shen, M. J. Graham, K. U. Jeong, H. Huang, D. Zhang, M. Guo, F. W. Harris, S. Z. D. Cheng, C. Y. Li and L. Zhu, *Chem. Mater.*, 2004, **16**, 1014–1025.
54 G. Wang, X. Tong and Y. Zhao, *Macromolecules*, 2004, **37**, 8911–8917.
55 H. Akiyama and N. Tamaoki, *Macromolecules*, 2007, **40**, 5129–5132.